

# The distribution and physical properties of high-redshift [OIII] emitters in a cosmological hydrodynamics simulation

Kana Moriwaki<sup>1\*</sup>, Naoki Yoshida<sup>1,2,3</sup>, Ikkoh Shimizu<sup>4</sup>, Yuichi Harikane<sup>1,5</sup>,  
Yuichi Matsuda<sup>6,7</sup>, Hiroshi Matsuo<sup>6,7</sup>, Takuya Hashimoto<sup>6,8</sup>, Akio K. Inoue<sup>8</sup>,  
Yoichi Tamura<sup>9</sup>, Tohru Nagao<sup>10</sup>.

<sup>1</sup>*Department of Physics, The University of Tokyo, 7-3-1 Hongo, Bunkyo, Tokyo 113-0033, Japan*

<sup>2</sup>*Kavli Institute for the Physics and Mathematics of the Universe (WPI), UT Institutes for Advanced Study, The University of Tokyo, 5-1-5 Kashiwanoha, Kashiwa, Chiba 277-8583, Japan*

<sup>3</sup>*Research Center for the Early Universe, School of Science, The University of Tokyo, 7-3-1 Hongo, Bunkyo, Tokyo 113-0033, Japan*

<sup>4</sup>*Theoretical Astrophysics, Department of Earth and Space Science, Osaka University, 1-1 Machikaneyama, Toyonaka, Osaka 560-0043, Japan*

<sup>5</sup>*Institute for Cosmic Ray Research, The University of Tokyo, 5-1-5 Kashiwanoha, Kashiwa, Chiba 277-8582, Japan*

<sup>6</sup>*National Astronomical Observatory of Japan, 2-21-1 Osawa, Mitaka, Tokyo 181-8588, Japan*

<sup>7</sup>*Department of Astronomical Science, School of Physical Sciences, The Graduate University for Advanced Studies (SOKENDAI), Osawa 2-21-1, Mitaka, Tokyo 181-8588, Japan*

<sup>8</sup>*Department of Environmental Science and Technology, Faculty of Design Technology, Osaka Sangyo University, 3-1-1, Nagaito, Daito, Osaka 574-8530, Japan*

<sup>9</sup>*Division of Particle and Astrophysical Science, Graduate School of Science, Nagoya University, Furo-cho, Chikusa-ku, Nagoya 464-8602, Japan*

<sup>10</sup>*Research Center for Space and Cosmic Evolution, Ehime University, 2-5 Bunkyo-cho, Matsuyama, Ehime 790-8577, Japan*

## ABSTRACT

Recent observations with the Atacama Large Millimeter/submillimeter Array (ALMA) detected far-infrared emission lines such as the [OIII] 88  $\mu\text{m}$  line from galaxies at  $z \sim 7 - 9$ . Far-infrared lines can be used to probe the structure and kinematics of such high-redshift galaxies as well as to accurately determine their spectroscopic redshifts. We use a cosmological simulation of galaxy formation to study the physical properties of [OIII] 88  $\mu\text{m}$  emitters. In a comoving volume of 50  $h^{-1}$  Mpc on a side, we locate 34 galaxies with stellar masses greater than  $10^8 M_\odot$  at  $z = 9$ , and more than 270 such galaxies at  $z = 7$ . We calculate the [OIII] 88  $\mu\text{m}$  luminosities ( $L_{\text{OIII},88}$ ) by combining a physical model of HII regions with emission line calculations using the photoionization code CLOUDY. We show that the resulting  $L_{\text{OIII},88}$ , for a given star formation rate, is slightly higher than predicted from the empirical relation for local galaxies, and is consistent with recent observations of galaxies at redshifts 7 - 9. Bright [OIII] emitters with  $L_{\text{OIII},88} > 10^8 L_\odot$  have stellar masses greater than  $10^9 M_\odot$ , star formation rates higher than  $3 M_\odot \text{yr}^{-1}$ , and the typical metallicity is  $\sim 0.1 Z_\odot$ . The galaxies are hosted by dark matter halos with masses greater than  $10^{10.5} M_\odot$ . Massive galaxies show characteristic structure where the [OIII] emitting gas largely overlaps with young stars, but the emission peak is separated from the main stellar population, suggesting the stochastic and localized nature of star formation in the first galaxies. We propose to use the [OIII] 5007Å line, to be detected by James Webb Space Telescope (JWST), to study the properties of galaxies whose [OIII] 88 $\mu\text{m}$  line emission has been already detected with ALMA. The large-scale distribution of [OIII] 5007Å emitters can be probed by using JWST NIRC2, and by proposed future space missions such as SPHEREx and CDIM.

**Key words:** galaxies: evolution — galaxies: high-redshift — galaxies: ISM

## 1 INTRODUCTION

One of the major goals of the next generation space-borne and ground-based telescopes is to detect and characterize

\* E-mail: kana.moriwaki@utap.phys.s.u-tokyo.ac.jp

the first galaxies that were in place several hundred million years after the Big Bang. There has been impressive progress in exploration of the redshift frontier of distant galaxies. Hubble Space Telescope have detected a number of distant galaxies by dropout techniques (Yan et al. 2011; Ellis et al. 2013; McLeod et al. 2013; Schenker et al. 2013; Dunlop et al. 2013; Robertson et al. 2013; Ono et al. 2013; Koekemoer et al. 2013; Oesch et al. 2013; Bouwens et al. 2014; Finkelstein et al. 2014; Bouwens et al. 2015). Intrinsically faint galaxies have also been detected with the help of gravitational lensing magnification (Zheng et al. 2012; Oesch et al. 2014; Ishigaki et al. 2015). Hydrogen Ly $\alpha$  line has been used primarily to determine the spectroscopic redshifts of these galaxies. Unfortunately, the Ly $\alpha$  line becomes increasingly weak at  $z > 7$  through the epoch of reionization when the IGM neutral fraction increases (e.g. Konno et al. 2014).

Rest-frame far-infrared lines are promising probe of distant galaxies. The Atacama Large Millimeter/submillimeter Array (ALMA) is capable of detecting multiple far-infrared lines even from galaxies at  $z > 7$ . Although initial attempts to detect the [CII] 158 $\mu$ m line, one of the brightest emission lines from star-forming galaxies, resulted in both success and non-detections (Walter et al. 2012; Kaneker et al. 2013; Ouchi et al. 2013), recent observations show that the [CII] 158 $\mu$ m line can be used to identify and to study the structure and kinematics of distant galaxies (Smit et al. 2018).

[OIII] 88 $\mu$ m emission is another excellent probe of high-redshift star-forming galaxies. From a theoretical point of view, the [OIII] 88 $\mu$ m emission is easy to model because it originates from HII regions, unlike the [CII] 158 $\mu$ m emission which likely originates from both ionized and neutral regions (Nagamine et al. 2006; Pallottini et al. 2017; Lagache et al. 2018). Interestingly, many nearby dwarf galaxies show stronger [OIII] 88 $\mu$ m emission than [CII] 158 $\mu$ m (Madden et al. 2012; Leboutteiller et al. 2012; Cormier et al. 2015). Motivated by these observations, Inoue et al. (2014) proposed to use the [OIII] 88 $\mu$ m line to determine the spectroscopic redshifts of galaxies at  $z > 8$ . Recent observations using ALMA successfully discovered the [OIII] line from galaxies beyond redshift 7 (Inoue et al. 2016; Carniani et al. 2017; Laporte et al. 2017) and even at  $z = 9.11$  (Hashimoto et al. 2018a). In combination with optical/infrared observations and detection of the hydrogen Lyman- $\alpha$  line, the ALMA observations provide rich information on the physical properties of the early galaxies that are thought to have driven cosmic reionization.

With the launch of James Webb Space Telescope (JWST) scheduled in 2020, it is timely and important to study the formation and evolution of early emission line galaxies. To this end, we use a high-resolution cosmological simulation of galaxy formation and study the statistics and physical properties of a population of [OIII] emitters at  $z > 7$ . Throughout the present Letter, we adopt a  $\Lambda$ CDM cosmology with the matter density  $\Omega_M = 0.3175$ , the cosmological constant  $\Omega_\Lambda = 0.6825$ , the Hubble constant  $h = 0.6711$  in units of  $H_0 = 100 \text{ km s}^{-1} \text{ Mpc}^{-1}$  and the baryon density  $\Omega_B = 0.04899$ . The matter density fluctuations are normalized by setting  $\sigma_8 = 0.8344$  (Planck Collaboration 2014).

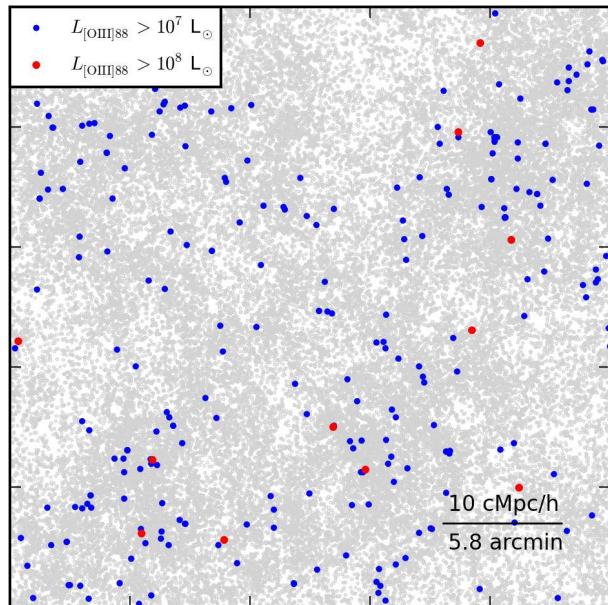


**Figure 1.** We plot the projected distribution of [OIII] emitters at  $z = 7$  in a cubic volume of comoving  $50 h^{-1} \text{ Mpc}$  ( $= 29''$ ) on a side. The gray points are all the galaxies in this volume, whereas the blue and red points represent galaxies with  $L_{\text{OIII},88} > 10^7 L_\odot$  and  $> 10^8 L_\odot$ , respectively. The [OIII] 5007 $\text{\AA}$  line luminosities can be approximately estimated by multiplying  $L_{\text{OIII},88}$  by a factor of ten.

## 2 METHODS

We use outputs of a cosmological hydrodynamics simulation of Shimizu et al. (2016). The simulation follows the formation of galaxies in a fully cosmological context by implementing star formation, the stellar feedback effects by radiation pressure and supernova explosions, and multi-element chemical enrichment (Okamoto et al. 2008, 2010, 2014; Okamoto & Frenk 2009). Our simulation reproduces a broad range of the observed features of high-redshift galaxy populations such as Lyman break galaxies, Lyman- $\alpha$  emitters, and sub-mm galaxies as well as those of local galaxies (Shimizu et al. 2012, 2014, 2016; Okamoto et al. 2014). The details of the simulation are found in Shimizu et al. (2016). The initial conditions are configured with  $2 \times 1280^3$  gas and dark matter particles in a cubic volume of comoving  $50 h^{-1} \text{ Mpc}$ . The mass of a dark matter particle is  $4.44 \times 10^6 h^{-1} M_\odot$  and the initial mass of a gas particle is  $8.11 \times 10^5 h^{-1} M_\odot$ . The softening length for the gravitational force is set to be  $2 h^{-1} \text{ kpc}$  in comoving unit.

Following the standard star-formation prescription, star particles are spawned in cold and dense gas clouds. The mass of a star particle is as small as  $\sim 10^6 M_\odot$ , and thus galaxies with mass  $\sim 10^9 M_\odot$  are represented by more than  $\sim 1000$  star particles and gas particles. We study the internal structure of the galaxies of sub-kpc scales such as the relative distributions of young and old stars, and also the distribution of rest-frame optical/far-infrared line emitting regions.

**Table 1.** The parameters used to calculate the line luminosities with CLOUDY. The metallicities are normalized by  $Z_{\odot} = 0.02$ .

$\log_{10}(Z/Z_{\odot})$	-2.2, -1.6, -0.6, -0.3, 0.1, 0.5
$\log_{10} U$	-4.0, -3.9, ..., -1.1, -1.0
$\log_{10}(n/\text{cm}^{-3})$	1.0, 2.0, 3.0

### 3 SPECTRAL ENERGY DISTRIBUTION OF GALAXIES

We calculate the SED of each spawned star particle using the population synthesis code PÉGASE2 (Fioc & Rocca-Volmerange 1997). We obtain the total SED of a simulated galaxy by summing the contributions from all the star particles within the galaxy. We adopt the Calzetti law of dust extinction (Calzetti et al. 2000). We calculate the escape probability  $f_{\text{UV}}$  of ultra-violet (UV) photons at 1500 Å adopting a dust distribution model of Xu & Buat (1995) and Shimizu et al. (2014):

$$f_{\text{UV}} = \frac{1 - \delta}{2}(1 + e^{-\tau_d}) + \frac{\delta}{\tau_d}(1 - e^{-\tau_d}), \quad (1)$$

where  $\delta$  is a parameter whose value is from 0 to 1 and  $\tau_d$  is the UV optical depth. The optical depth  $\tau_d$  is calculated in the same way as in Shimizu et al. (2016). With  $\delta = 0.95$  for attenuation of continuum, the rest-frame UV luminosity function matches well to the observed ones at  $z = 6 - 10$ .

The nebular emission line luminosities are calculated in the following manner. We assume that the line luminosity,  $L_{\text{line}}$ , is proportional to the H $\beta$  luminosity with the case-B approximation (Dopita & Sutherland 2003),  $L_{\text{H}\beta}^{\text{caseB}}$ , as

$$L_{\text{line}} = (1 - f_{\text{esc}})C_{\text{line}}(Z, \langle U \rangle, n_{\text{H}})L_{\text{H}\beta}^{\text{caseB}}, \quad (2)$$

where  $f_{\text{esc}}$  is the Lyman continuum escape fraction and  $C_{\text{line}}$  is the line luminosity ratio. We generate a library of emission lines using CLOUDY (Ferland et al. 2013) following Inoue (2011) and Inoue et al. (2014). The library covers a wide range of gas metallicity  $Z$ , the ionization parameter  $\langle U \rangle$  and the gas density  $n_{\text{H}}$  as given in Table 1. We assume  $f_{\text{esc}} = 0.1$  in the present Letter.

Individual HII regions are not resolved in our simulation, and thus we resort to a simple physical model of the inter-stellar medium (ISM) structure to calculate the emissivities of the lines originating from HII regions. We characterize the ISM by the local density  $n_{\text{H}}$  and metallicity  $Z$ , and also by a volume-averaged ionization parameter

$$\langle U \rangle = \frac{3\alpha_{\text{B}}^{2/3}}{4c} \left( \frac{3\langle Q \rangle n_{\text{H}}}{4\pi} \right)^{1/3}, \quad (3)$$

where  $\langle Q \rangle$  is the production rate of ionizing photons from each star particle, and  $\alpha_{\text{B}}$  is the case-B hydrogen recombination coefficient. Essentially, we assume a constant gas density in a spherical HII region surrounding a star particle (e.g. Panuzzo et al. 2003; Hirschmann et al. 2017). We assume that the gas density of the HII region surrounding the star particles scales with the global gas density  $\langle n_{\text{H}} \rangle$ , which is calculated from the half stellar-mass radius of the galaxy and the gas mass within it, as  $n_{\text{H}} = K \langle n_{\text{H}} \rangle$ . With  $K = 5$  as our fiducial value, the HII region density ranges approximately from 30 to 300  $\text{cm}^{-3}$ , which is the typical range of the nearby HII region density (Osterbrock & Ferland 2006).

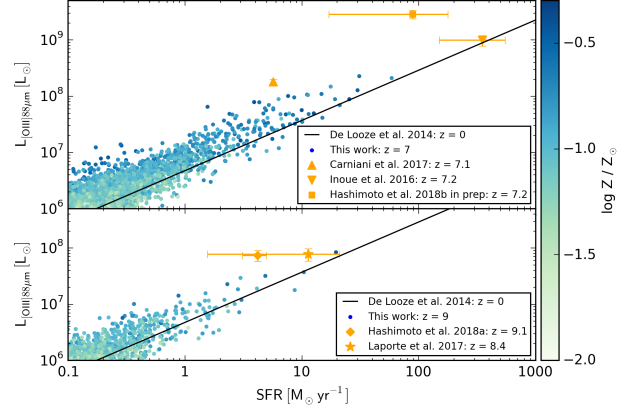


**Figure 2.** The [OIII] line luminosity against star formation rate of our galaxy samples at  $z = 7$  and  $z = 9$ . We indicate the gas metallicity by the color of each point. We compare them with the observed galaxies at  $z = 7 - 9$  (Inoue et al. 2016; Carniani et al. 2017; Laporte et al. 2017; Hashimoto et al. 2018a,b). The black line shows the [OIII]-SFR relation derived by De Looze et al. (2014) for all kinds of local galaxies.

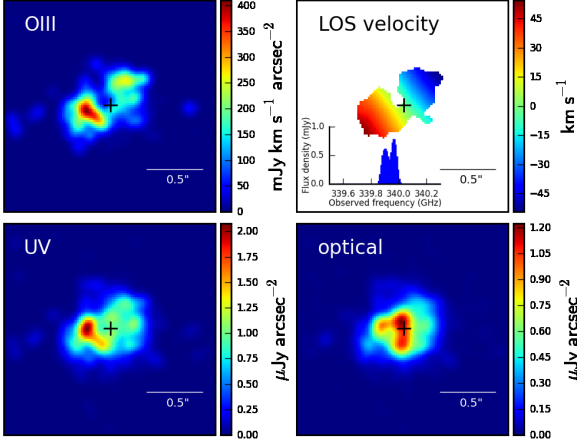
### 4 RESULTS

Figure 1 shows the spatial distribution of the [OIII] emitters identified at  $z = 7$ . The blue and red points represent galaxies with  $L_{\text{OIII},88} > 10^7 L_{\odot}$  and  $> 10^8 L_{\odot}$ , respectively. The [OIII] emitters are strongly clustered, and trace the large-scale structure of  $\sim 10 h^{-1} \text{Mpc}$  scales. The early large-scale structure and its evolution can be probed by future observations with JWST NIRCам targeting rest-frame optical emission lines such as [OIII] 5007Å, as we propose in Discussion section, or by utilizing the intensity mapping technique at sub-millimeter wavelengths (Visbal & Loeb 2010). Our simulation predicts that the total [OIII] 88 $\mu\text{m}$  luminosity at  $z = 7$  in a cubic volume of comoving  $50h^{-1} \text{Mpc}$  is  $2.0 \times 10^{10} L_{\odot}$ , giving a significant contribution to the global sub-millimeter line intensity.

In Figure 2, we plot  $L_{\text{OIII},88}$  against star-formation rate (SFR) for our emission line galaxy samples. For reference, we also show the  $L_{\text{OIII},88}$ -SFR relation for all kinds of local galaxies derived by De Looze et al. (2014). Our model predicts slightly larger values of  $L_{\text{OIII},88}$  than the local relation; early galaxies tend to be compact and have large ionization parameters. Several galaxies in the simulated volume have  $L_{\text{OIII},88}$  and SFRs comparable to the intrinsic  $L_{\text{OIII},88}$  and SFRs of the galaxies recently identified at  $z \sim 7 - 9$  (Carniani et al. 2017; Laporte et al. 2017; Hashimoto et al. 2018a). The bright [OIII] emitters have a metallicity of  $\sim 0.1 Z_{\odot}$ , consistent with the estimate of, e.g., Inoue et al. (2016). The [OIII] emitters with  $L_{\text{OIII},88} > 10^8 L_{\odot}$  at  $z = 7$  are hosted by dark matter halos with more massive than  $10^{10.5} M_{\odot}$ , and their strong clustering pattern is clearly seen in Figure 1. These features suggest that the [OIII] 88 $\mu\text{m}$  emitters at  $z \sim 7 - 9$  represent relatively well-established galaxies in the early universe.

The bright [OIII] emitters have extended structure of  $\sim 1 \text{kpc}$ . We find that the [OIII] 88 $\mu\text{m}$  emitting regions in the galaxies are highly localized and often displaced from the bulk stellar distribution. Figure 3 shows the structure of one of the brightest galaxies at  $z = 9$ . Motivated by





**Figure 3.** The structure of a galaxy at  $z = 9$  with  $M_* = 6.3 \times 10^8 M_\odot$ ,  $M_{\text{halo}} = 2.1 \times 10^{10} M_\odot$ ,  $\text{SFR} = 5.9 M_\odot/\text{yr}$ , and  $L_{\text{OIII},88} = 2.2 \times 10^7 L_\odot$ . We plot the [OIII]  $88\mu\text{m}$  flux, the [OIII] luminosity weighted line-of-sight gas velocity, the rest-frame UV continuum ( $1600 \text{ \AA}$ ) flux and the rest-frame optical continuum ( $5000 \text{ \AA}$ ) flux. The cross indicate the mass center of the stars. For this figure, we assume that the galaxy is gravitationally lensed with  $\mu = 10$ , to be compared with, e.g., MACS1149-JD1 (Hashimoto et al. 2018a). The inset of the upper right panel shows the spectrum to be observed with ALMA.

the intriguing observation of a gravitationally lensed galaxy MACS1149-JD1 (Hashimoto et al. 2018a), we generate Figure 3 assuming an isotropic lensing magnification of  $\mu = 10$ . With the help of lensing, the effective physical resolution increases by a factor of  $\sim 3$ .

Both of the [OIII]  $88\mu\text{m}$  line emission and the UV continuum trace young stellar populations with ages shorter than several million years. Though the relative displacement between the two distributions is often found for our bright galaxy samples, the flux peaks roughly coincide with each other, consistent with the observed galaxies at  $z \sim 7 - 9$  (Inoue et al. 2016; Hashimoto et al. 2018a). We note that there can also be spacial offsets between the [OIII]  $88\mu\text{m}$  and the UV emission caused by an inhomogeneous dust distribution (Katz et al. 2017).

## 5 DISCUSSION

Conventional optical line diagnostics can be used to study the physical properties of the early star-forming galaxies. We calculate the [OIII]  $5007\text{\AA}$  luminosity function and compare it with the luminosity function of [OIII]  $88\mu\text{m}$  (Figure 4). The vertical lines in the figure indicate typical detection limits of ALMA and JWST. As expected, the [OIII]  $5007\text{\AA}$  luminosity is roughly an order of magnitude larger than that of [OIII]  $88\mu\text{m}$ . Clearly, JWST can detect [OIII]  $5007\text{\AA}$  line emission from the galaxies whose [OIII]  $88\mu\text{m}$  lines (will) have been detected with ALMA.

The superb spectral and angular resolution of JWST NIRSpec IFU spectroscopy will enable us to study the structure and the kinematics of galaxies at  $z > 7$ . Gravitational lensing greatly helps not only by increasing the apparent flux of distant galaxies, but also by increasing the effec-

tive ‘physical’ spatial resolution. The sub-arcsecond resolutions of ALMA and JWST can be fully exploited to study the fine structure of lensed galaxies even at sub-kiloparsec scales. Signatures of merger event or the galaxy’s rotation can also appear as the line-of-sight velocity gradient of typically  $\Delta v \sim 100 \text{ km s}^{-1}$  (see the upper-right panel of Figure 3).

Future observations with ALMA and JWST hold promise to understand the formation and evolution of the first galaxies. Combining with fully resolved observations of other rest-frame optical and far-infrared emission lines originating from hydrogen, carbon and oxygen in a variety of phases in the ISM, and also with dust continuum emission, we will be able to study the chemical evolution and the ISM structure and kinematics of the galaxies a few to several hundred million years after the Big Bang. It is important to explore theoretically pan-chromatic approaches to elucidate the nature of the first galaxies.

The large-scale distribution of the [OIII] emitters can be probed by using JWST NIRCcam, either by using its narrow band filters or with its grism spectroscopy mode. For instance, the line sensitivity for the NIRCcam grism module at the F444W band is  $\sim 3.4 \times 10^{-18} \text{ erg s}^{-1} \text{ cm}^{-2}$  for  $\text{S/N} = 5$  with a  $10^4$  second exposure. It is expected from Figure 1 and 4 that, within the field-of-view of  $2 \times 2.2' \times 2.2'$ , there will be several [OIII]  $5007\text{\AA}$  emitters on average detected in the redshift range of  $6.8 < z < 9.0$ . Multiple pointings or mosaic observations will map the three-dimensional distribution of [OIII] emitters in the redshift range.

Systematic surveys with JWST NIRCcam narrow-bands can also probe the large-scale structure at  $z > 8$ . If we perform a narrow-band survey using the F466N filter with the same exposure, we can detect, with  $\text{S/N} = 5$ ,  $z = 8.3$  [OIII] emitters with line fluxes above  $\sim 6.6 \times 10^{-19} \text{ erg s}^{-1} \text{ cm}^{-2}$ . This limit roughly corresponds to detecting the galaxies shown by blue points in Figure 1. In such narrow-band surveys, foreground  $\text{H}\alpha$  emitters are severe contaminants, or can actually be major targets at the corresponding wavelength (Silva et al. 2018), but one can use  $J$ -dropout technique to select [OIII]  $5007\text{\AA}$  emitters. We have found that the [OIII] emitters at  $z = 8.3$  in our simulation are separated typically by  $Y_{105} - J_{125} > 1.0 - 1.5$  from  $\text{H}\alpha$  emitters at  $z = 6.2$ . It is possible to select preferentially the [OIII] emitters if we choose and survey a region where deep broad-band data are available.

Future space missions such as Spectrophotometer for the History of the Universe, Epoch of Reionization, and Ice Explorer (SPHEREx) and Cosmic Dawn Intensity Mapper (CDIM) utilize the infrared intensity mapping technique to probe the large-scale galaxy distribution at high-redshifts (Cooray et al. 2016; Dore et al. 2016). Redshifted [OIII]  $5007\text{\AA}$  emission from early star-forming galaxies such as those studied in the present Letter is an excellent target, and thus serve as a valuable cosmological probe.

## ACKNOWLEDGMENTS

This research was supported by the Munich Institute for Astro- and Particle Physics (MIAPP) of the DFG cluster of excellence ‘‘Origin and Structure of the Universe’’. K.M. has been supported by Advanced Leading Graduate Course

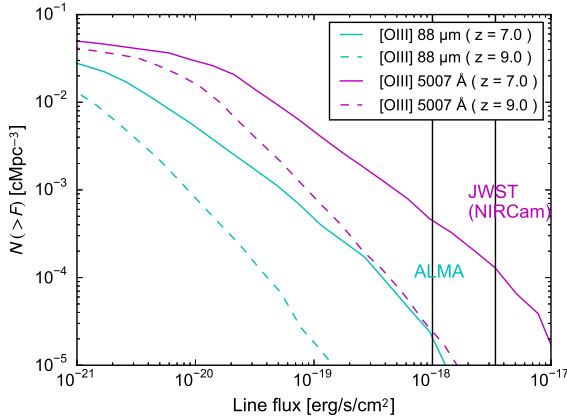


**Figure 4.** The cumulative line luminosity function for [OIII] 88 $\mu$ m (cyan lines) and [OIII] 5007 Å (magenta lines). The solid lines and the dotted lines show the data of  $z = 7$  and  $z = 9$  respectively. Vertical lines represent typical detection limit of ALMA and that of JWST NIRCcam assuming  $10^4$  second integration and the signal-to-noise ratio of 5.

for Photon Science (ALPS) of the University of Tokyo. Y.H., Y.M., A.K.I. and Y.T. acknowledge JSPS KAKENHI grants 16J03329 (Y.H.), 17H04831, 17KK0098 (Y.M.), 17H01114 (A.K.I) and 17H06130 (Y.T). T.H., A.K.I and Y.T. acknowledge the NAOJ ALMA Scientific Research Grand number 2016-01A (T.H.), 2016-01A (A.K.I) and 2018-09B (Y.T.).

## REFERENCES

Bouwens, R. J., Illingworth, G. D., Oesch, P. A., et al. 2014, *ApJ*, 793, 115  
 Bouwens, R. J., Illingworth, G. D., Oesch, P. A., et al. 2015, *ApJ*, 803, 34  
 Calzetti, D., Armus L., Bohlin, R. C., et al. 2000, *ApJ*, 533, 682  
 Carniani, S., Maiolino, R., Pallottini, A., et al. 2017, *A&A*, 605, A42  
 Cooray, A., et al. 2016, arXiv:1602.05178  
 Cormier, D., Madden, S. C., Leboutteiller, V., et al. 2015, *A&A*, 578, A53  
 De Looze, I., Cormier, D., Leboutteiller, V., et al. 2014, *A&A*, 568, A62  
 Dunlop, J. S., Rogers, A. B., McLure, R. J., et al. 2013, *MNRAS*, 432, 3520  
 Dopita M. A., Sutherland R. S., 2003, *Astrophysics of the diffuse universe*  
 Dore, O., et al. 2016, arXiv:1606.07039  
 Ellis, R. S., McLure, R. J., Dunlop, J. S., et al. 2013, *ApJ*, 763, L7  
 Ferland, G. J., Porter, R. L., van Hoof, P. A. M., et al. 2013, *RMxAA*, 49, 137  
 Finkelstein, S. L., Ryan, Jr., R. E., Papovich, C., et al. 2014, arXiv:1410.5439  
 Fioc, M., & Rocca-Volmerange, B. 1997, *A&A*, 326, 950  
 Hashimoto, T., Laporte, N., Mawatari, K., et al. 2018, *Nature*, 557, 392  
 Hashimoto, T. et al. 2018, to be submitted to *PASJ*

Hirschmann, M., Charlot, S., Feltre, A., et al. 2017, arXiv:1706.00010v2  
 Inoue, A. K. 2011, *MNRAS*, 415, 2920  
 Inoue, A. K., Shimizu, I., Tamura, Y., et al. 2014, *ApJ*, 780, L18  
 Inoue, A. K., Tamura, Y., Matsuo, H., et al. 2016, *Science*, 352, 1559  
 Ishigaki, M., Kawamata, R., Ouchi, M., et al. 2015, *ApJ*, 799, 12  
 Kaneker, N., Wagg, J., Ram Chary, R., & Carilli, C. 2013, *ApJL*, 771, L20  
 Katz, H., Kimm, T., Sijacki, D., Haehnelt, M. G., 2017, *MNRAS*, 468, 4831  
 Koekemoer, A. M., Ellis, R. S., McLure, R. J., et al. 2013, *ApJS*, 209, 3  
 Konno, A., Ouchi, M., Ono, Y., et al. 2014, *ApJ*, 797, 16  
 Leboutteiller, V., Cormier, D., Madden, F., et al. 2012, *A&A*, 548, A91  
 Lagache, G., Cousin, M., Chatzikos, M. 2018, *A&A*, 609, 130  
 Laporte, N., Ellis, R. S., Bauer, F. E., et al. 2017, *ApJ*, 837, L21  
 Leitherer, C., Schaerer, D., Goldader, J. D., et al. 1999, *ApJS*, 123, 3  
 Madden, S. C., Rémy, A., Galliano, F., et al. 2012, in *IAU Symp. 284, The Spectral Energy Distribution of Galaxies*, ed. R. J. Tuffs & C. C. Popescu (Cambridge: Cambridge Univ. Press), 141  
 McLeod, D. J., McLure, R. J., Dunlop, J. S., 2016, *MNRAS*, 459, 3812  
 Nagamine, K., Wolfe, A. M., Hernquist, L. H., 2006, *ApJ*, 647, 60  
 Oesch, P. A., Bouwen, R. J., Illingworth, G. D., et al., 2013, *ApJ*, 773, 75  
 Oesch, P. A., Bouwen, R. J., Illingworth, G. D., et al., 2014, arXiv:1409.1228  
 Okamoto, T., Frenk, C. S., Jenkins, A., Theuns, T. 2010, *MNRAS*, 406, 208  
 Okamoto, T., Frenk, C. S., 2009, *MNRAS*, 399, 174  
 Okamoto, T., Nemmen, R. S., Bower, R. G., 2008, *MNRAS*, 385, 161  
 Okamoto, T., Shimizu, I., Yoshida, N., 2014, *PASJ*, 66, 70  
 Ono, Y., Ouchi, M., Curtis-Lake, E., et al., 2013, *ApJ*, 777, 155  
 Osterbrock D. E., Ferland G. J., 2006, *Astrophysics of Gaseous Nebulae and Active Galactic Nuclei*  
 Ouchi, M., Ellis, R., Ono, Y., et al. 2013, *ApJ*, 778, 102  
 Pallottini, A., Ferrara, A., Gallerani, S., Vallini, L., Maiolino, R., Salvadori, S., 2017, *MNRAS*, 465, 2540  
 Panuzzo, P., Bressan, A., Granato, G. L., et al. 2003, *A&A*, 409, 99  
 Planck Collaboration., 2014, *A&A*, 571, 16  
 Robertson, B. E., Furlanetto, S. R., Schneider, E., et al. 2013, *ApJ*, 768, 71  
 Schenker, M. A., Robertson, B. E., Ellis, R. S., et al. 2013, *ApJ*, 768, 196  
 Shimizu, I., Inoue, A. K., Okamoto, T., Yoshida, N., 2014, *MNRAS*, 440, 731  
 Shimizu, I., Inoue, A. K., Okamoto, T., Yoshida, N. 2016, *MNRAS*, 461, 3563  
 Shimizu, I., Yoshida, N., Okamoto, T., 2012, *MNRAS*, 427, 2866

- Silva, M. B., Zaroubi, S., Kooistra, R., Cooray, A., 2018, MNRAS, 475, 1587
- Smit, R, Bouwens, R. J., Carniani, S. et al. 2018, Nature, 553, 178
- Visbal, E. & Loeb, A. 2010, JCAP, 11, 016
- Walter, F., Decarli, R., Carilli, C., et al. 2012, ApJ, 752, 93
- Xu, C., Buat, V., 1995, A&A, 293, L65
- Yan, H., Yan, L., Zamojski, A. M., et al. 2011, ApJL, 728, L22
- Zheng, W., Postman, M., Zitrin, A., et al., 2012, Nature, 489, 406